https://doi.org/10.20965/ijat.2021.p0475

Paper:

Machinability Investigation for Cellulose Nanofiber-Reinforced Polymer Composite by Ultraprecision Diamond Turning

Yu Kamada and Jiwang Yan[†]

Department of Mechanical Engineering, Faculty of Science and Technology, Keio University
3-14-1 Hiyoshi, Kohoku-ku, Yokohama, Kanagawa 223-8522, Japan
[†]Corresponding author, E-mail: yan@mech.keio.ac.jp
[Received February 5, 2021; accepted May 17, 2021]

Cellulose nanofiber (CeNF)-reinforced polymer composites have wide potential applications in the manufacturing of optical and mechanical parts owing to their light weight, high mechanical strength, and optical transparency. In this study, CeNF-reinforced homogeneous polypropylene (PP-CeNF) was machined under various conditions by ultraprecision diamond turning, and the results were compared with those of pure PP without CeNF addition. The influence of CeNFs on material removal was investigated by examining the surface topography, chip morphology, cutting forces, and cutting temperature. It was found that the surface defects in pure PP cutting were surface tearing, while the surface defects of PP-CeNF were surface tearing and micro-holes induced by the pulling-outs of CeNFs. Surface tearing increased with cutting speed; pulling-outs of CeNFs were slightly affected by cutting speed but strongly dependent on the tool feed rate. Under a small tool feed rate, the surface roughness could be reduced to ∼10 nm *Ra* for PP-CeNF. The thermal effect was insignificant in the experiments, whereas the effect of strain rate-induced material hardening was dominant for both workpiece materials at a high cutting speed. This study helps to understand the mechanisms for ultraprecision cutting of CeNF-reinforced polymer composites and provides guidelines for improving the machined surface quality.

Keywords: polymer, ultraprecision cutting, cellulose nanofibers, composite material, surface defect

1. Introduction

Cellulose nanofiber (CeNF) is an attractive material for a variety of industrial applications, owing to its excellent properties such as high rigidity, light weight, low coefficient of thermal expansion, and optical transparency [1, 2]. Previous studies have shown that the elastic modulus of CeNF remains stable around 2–3 GPa at a temperature ranging from −200°C to 200°C [3, 4], and the linear thermal expansion coefficient of CeNF along the fiber direction is only 0.17 ppm/K [5].

Polymer reinforcement is one of the major applications of CeNF [6, 7]. Mixing the polymer with CeNF can improve the mechanical strength of the polymer; meanwhile, the transparency of the polymer will not be reduced [8]. Thus, polymer-CeNF composites are expected to be used for the manufacture of mechanical, optical, and electronic parts such as substrates for optical lenses, organic electroluminescence displays, and organic thin-film organic photovoltaics. Fujisawa et al. [9] reported that the elastic modulus and tensile strength of a non-crystalline polylactic acid (NPA) sheet containing 10% CeNF, which is made by a low-pressure forming process, are 1.3 times larger than those of the NPA sheet without CeNF addition. Researchers of the New Energy and Industrial Technology Development Organization (NEDO) [10] reported that they succeeded in improving the mechanical behavior of high-density polypropylene (HDPE) by mixing 10% CeNF. The elastic modulus and tensile strength of HDPE-CeNF were 4.5 times and 2.4 times, respectively, larger than those of HDPE, and the linear thermal expansion coefficient was decreased from 248 ppm/K (HDPE) to 47 ppm/K (HDPE-CeNF). Similar results were obtained for polypropylene (PP).

The shape formation of CeNF-reinforced polymer has been extensively studied. Injection molding is a commonly used processing method [11, 12]. However, it is difficult to fabricate high-precision parts with complex shapes because of the shape errors caused by thermal effects. This limits the application of polymer-CeNF composites in the optical field and other fields requiring high-precision parts. Alternatively, ultraprecision cutting may be a promising solution for fabricating complex shapes with a nanometric surface roughness on polymer-CeNF composites.

Several studies have been conducted on the ultraprecision cutting of fiber-reinforced materials. Yan et al. [13] investigated the effect of the fiber angle on the material removal mechanism of carbon-fiber-reinforced plastics (CFRP). They found that the finished surface roughness was maximized at a fiber angle of 90°, and tool wear increased as the fiber angle increased. Kaneeda [14] studied the effect of fiber direction on the cutting performance of CFRP and found that the roughness of the tool edge and the clearance angle affected the machinability. The amount of residual uncut and the depth of the damaged layer increased as the roundness of the tool edge in-

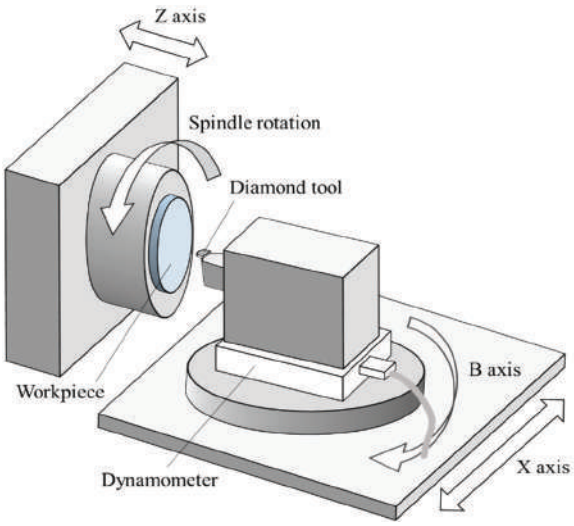

Fig. 1. Schematic diagram of experimental setup.

creased, and the amount of residual uncut and thrust force decreased as the clearance angle of the tool increased.

However, to date, there is no available literature on the cutting of polymer-CeNF composites; thus, its machinability is still unknown. Although there is some structural similarity between CFRP and polymer-CeNF, their sizes, distributions, and mechanical strengths are distinctly different. Carbon fibers are directional, with microscale diameters, whereas CeNFs are non-directional, with nanometric diameters. Therefore, the cutting performance of the polymer-CeNF composites should be different from that of CFRP.

In this study, ultraprecision diamond turning experiments were performed on polymer-CeNF composites to explore their micro/nanoscale machinability. In the experiments, CeNF-reinforced homogeneous polypropylene (PP) was used as the workpiece. The effects of CeNF on the surface topography, chip morphology, cutting force, and cutting temperature under various cutting conditions were examined. For comparison, pure PP without CeNF addition was also cut under the same conditions. This study aims to clarify the machinability of polymer materials containing CeNFs and contribute to the development of nanocomposite-based manufacturing.

2. Experimental Setup

The cutting experiments were carried out on a three-axis CNC ultraprecision lathe, NACHI ASP-15 (NACHI-FUJIKOSHI Corp., Japan). **Fig. 1** shows a schematic of the experimental setup. Pure PP without CeNF addition and PP containing 45%–55% CeNF (PP-CeNF) prepared by injection molding were used as the workpiece. The diameter of the CeNF was approximately 100 nm, and its length was several microns. The workpieces were 40 mm in diameter and 1.5 mm in thickness. A single-crystal diamond tool with a nose radius of

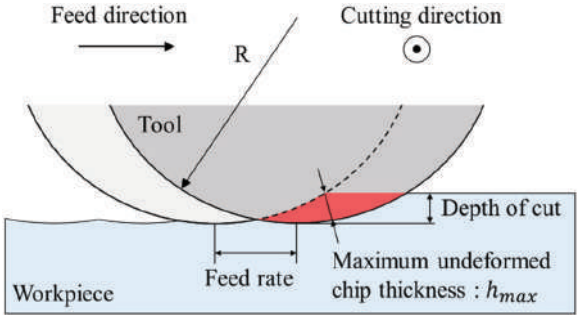

Fig. 2. Cutting model of a round-nosed diamond tool.

Table 1. Cutting conditions.

Parameters	Value
Cutting tool	Round-nosed diamond tool
Nose radius R	10 mm
Edge radius r	50 nm
Rake angle	0°
Flank angle	8°
Feed rate f	5, 30 μm/rev
Depth of cut d	10 μm
Spindle rotation rate N	2000 rpm
Cutting speed V	0–210 m/min
Cutting atmosphere	Dry

10 mm, a rake angle of 0°, and a flank angle of 8° was used. The edge radius of the diamond tool is approximately 50 nm [15]. **Fig. 2** shows the cutting model of a round-nosed diamond tool. The maximum undeformed chip thickness $h_{\max}$ can be expressed as follows [16]:

$$h_{\max} = R - \sqrt{R^2 + f^2 - 2f\sqrt{2Rd - d^2}}, \quad \ldots \quad (1)$$

where R is the tool nose radius, f is the tool feed rate, and d is the depth of the cut.

The cutting conditions are summarized in **Table 1**. The depth of cut d was set to 10 μm, so that the maximum undeformed chip thickness $h_{\max}$ varied in the range of 222–1296 nm when the tool feed rate f was changed from 5 to 30 μm/rev. These conditions are suitable for investigating material behavior at the micro/nanoscale level. The theoretical surface roughness calculated under this condition ranges from 0.3 to 11.3 nm Ry. The spindle rotation rate was set to 2000 rpm; thus, when the tool was fed from the outer edge of the workpiece to the workpiece center, the cutting speed varied from 210 to 0 m/min. During the cutting process, the cutting forces were measured using a three-component piezoelectric dynamometer (Kistler 9256C2). All experiments were performed under dry conditions to collect cutting chips for observation.

The machined surfaces and collected cutting chips were observed using a field-emission scanning electron microscope (FE-SEM) (ZEISS MERLIN Compact, Carl Zeiss AG). Then, the topographies of the machined surfaces

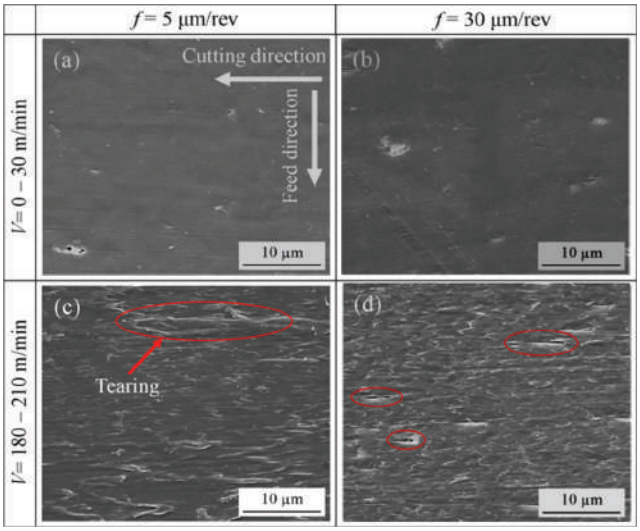

Fig. 3. SEM images of machined surfaces of pure PP at various tool feed rates and cutting speeds.

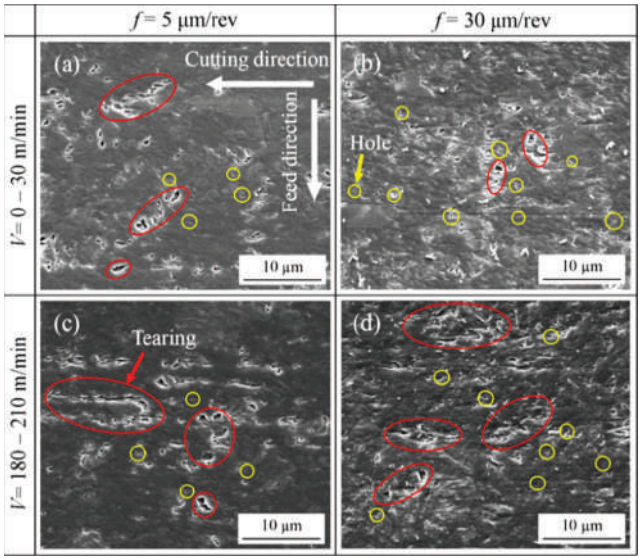

Fig. 4. SEM images of machined surfaces of PP-CeNF at various tool feed rates and cutting speeds.

were measured using a white light interferometer Talysurf CCI 1000 (AMETEK, Inc.). The cutting temperature was measured using an infrared thermography camera R550Pro (NIPPON AVIONICS Co., Ltd.).

3. Results and Discussion

3.1. Surface Topography and Chip Morphology

Figure 3 shows the machined surfaces of pure PP at various tool feed rates and cutting speeds. Under both feed rates of 5 and 30 μm/rev, the machined surfaces were smooth at a low cutting speed (V = 0–30 m/min), as shown in **Figs. 3(a)** and **(b)**. However, surface defects caused by material tearing are observed on the surfaces at a high cutting speed (V = 180–210 m/min), as indicated by the ellipses in **Figs. 3(c)** and **(d)**. These results indicate that the material removal behavior of pure PP is less affected by the tool feed rate but strongly dependent on the cutting speed.

Previous studies have shown that polymers have higher viscoelasticity and lower softening/melting temperatures than metals [17]. For pure PP, the softening point is 100°C–140°C [18–20]. Therefore, under a high cutting speed, if the temperature of the cutting region exceeds the softening point of pure PP, it may result in thermal softening [21], and in turn, reduce the cutting forces. On the other hand, polymers have low strain relaxation speeds. If stress relaxation occurs at a lower speed than the strain rate, which is determined by the cutting speed, the material hardness becomes higher than that under a low strain rate. In this case, a high cutting speed leads to a high cutting force [22]. As demonstrated by the measurement results of the cutting forces and temperatures in the following sections, the strain-rate-induced hardening effect was dominant.

Figure 4 shows the machined surfaces of PP-CeNF under the same conditions as those in **Fig. 3**. It can be observed from **Fig. 4** that submicron-scale surface tearing occurred even at a low cutting speed, which is different from the results obtained for pure PP (**Fig. 3**). This might be due to the fact that in the cutting process, some CeNFs were pulled out from the surface instead of being cut off. This can be proven by the presence of many micro-holes formed on the machined surfaces, as indicated by the circles in **Fig. 4**. To characterize the micro-holes, a high-magnification image of a typical machined surface of PP-CeNF was obtained, as shown in **Fig. 5**. The diameter of the micro-holes is a few tens of nanometers, which is close to the diameter of the CeNFs. The effect of CeNF on the material removal mechanism of the PP matrix will be discussed in Section 3.5.

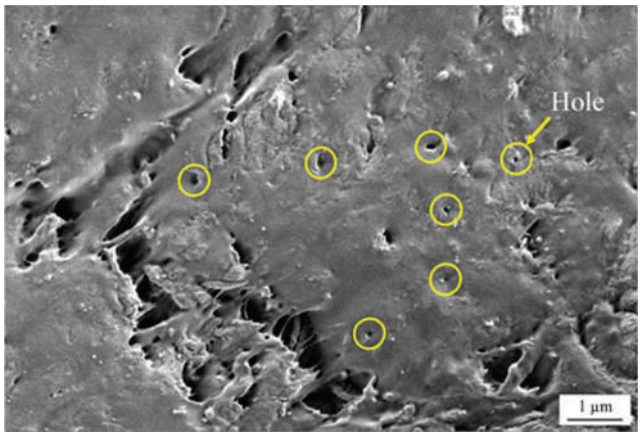

Fig. 5. Close-up view of the machined surface of PP-CeNF under f = 30 μm/rev.

On the other hand, it is clear that the flatness of the machined surfaces under a small feed rate (f = 5 μm/rev) shown in **Figs. 4(a)** and **(c)** are better than those at a high feed rate (f = 30 μm/rev), as shown in **Figs. 4(b)**

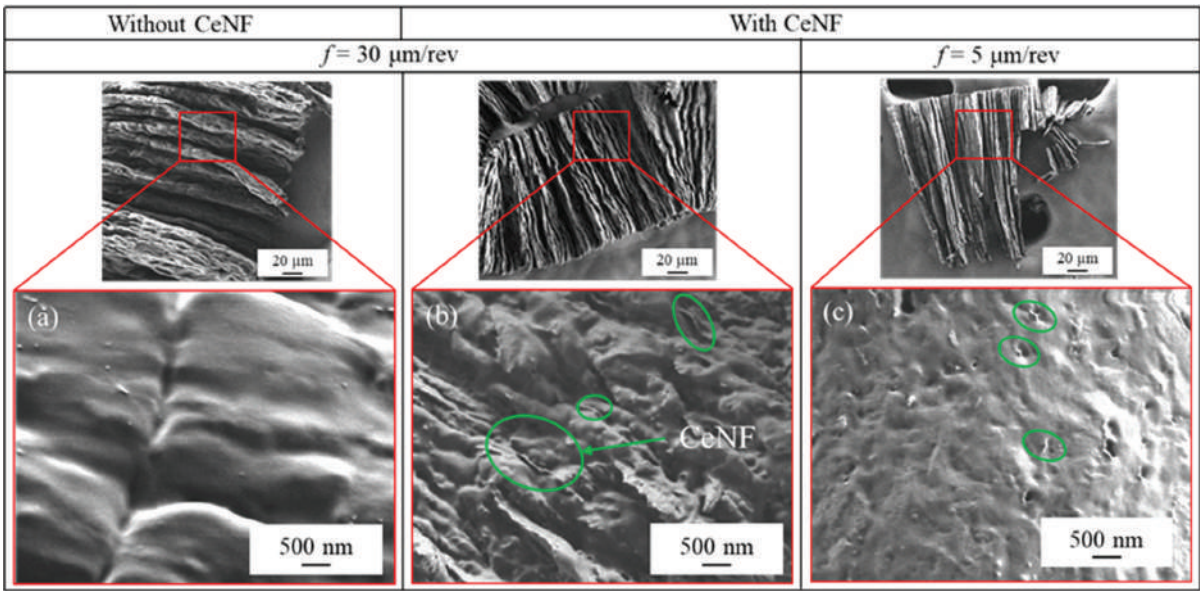

Fig. 6. SEM images of cutting chips: (a) pure PP at $f = 30$ μm/rev; (b) PP-CeNF at $f = 30$ μm/rev; (c) PP-CeNF at $f = 5$ μm/rev.

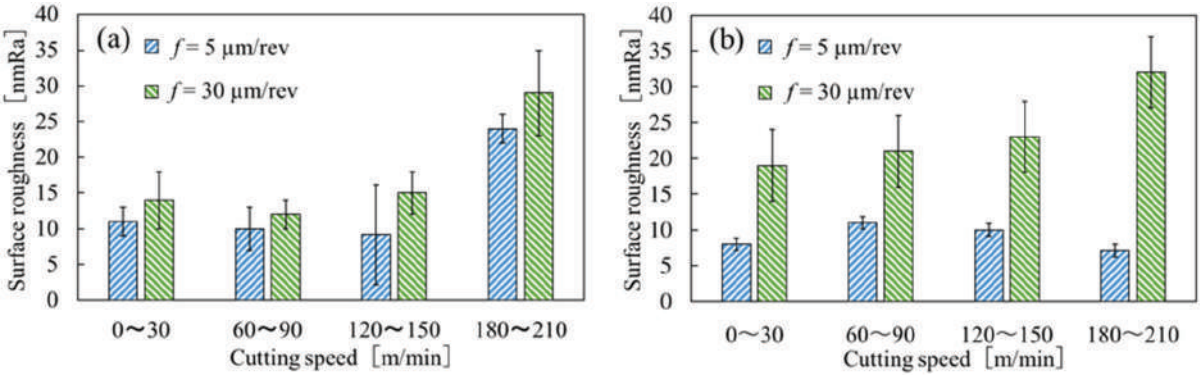

Fig. 7. Surface roughness of the machined workpieces: (a) pure PP; (b) PP-CeNF.

and **(d)**. Compared with the tool feed rate, the cutting speed had less effect on the surface quality of PP-CeNF. This might be because the tensile strength of PP-CeNF is larger than that of pure PP [23, 24]. Consequently, the viscoelasticity-induced tearing was suppressed at high cutting speeds. However, increasing the tool feed rate increased the chip thickness. The length of the CeNFs embedded inside the chip also increases, which eases the pulling-out of CeNFs from the surface. As a result, tearing becomes dominant when machining PP-CeNF at a high tool feed rate.

Figure 6 shows SEM images of the cutting chips collected when machining both pure PP and PP-CeNF at a cutting speed of $V = 180$–210 m/min. Generally, ribbon-like continuous cutting chips are generated under each cutting condition. This indicates that both pure PP and PP-CeNF were removed in a ductile regime. However, the cutting chips exhibited different features in a high-magnification view. For pure PP, the surface of the cutting chip ($f = 30$ μm/rev) was smooth without any holes, as shown in **Fig. 6(a)**. The cutting chips generated at a feed rate of 5 μm/rev were similar to those generated at a feed rate of 30 μm/rev, which is not shown. For PP-CeNF, at a high feed rate ($f = 30$ μm/rev), tearing defects were dominant on the chip surface, as shown in **Fig. 6(b)**. In addition, protruding CeNFs, which were pulled out from the PP matrix, were observed on the chip surface. On the other hand, at a low feed rate ($f = 5$ μm/rev), the chip surface was smoother than that at a high feed rate, as shown in **Fig. 6(c)**. However, it should be noted that there are many micro-holes on the chip surface with $f = 5$ μm/rev. This indicates that at a low feed rate, the CeNFs are easily pulled out from the chip surface.

3.2. Surface Roughness

Figure 7 displays the surface roughness of the machined workpieces of pure PP and PP-CeNF. For each workpiece, the surface roughness of four different regions that were machined at cutting speeds of 0–30 m/min, 60–90 m/min, 120–150 m/min, and 180–210 m/min, respectively, were measured. For all the cases, the surface

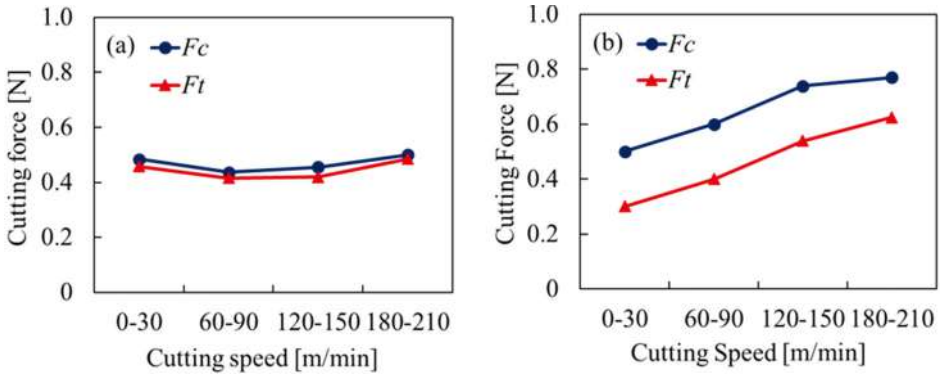

Fig. 8. Cutting forces of pure PP at various cutting speeds and feed rates: (a) $f = 5$ μm/rev; (b) $f = 30$ μm/rev (F_c: principal force, F_t: thrust force).

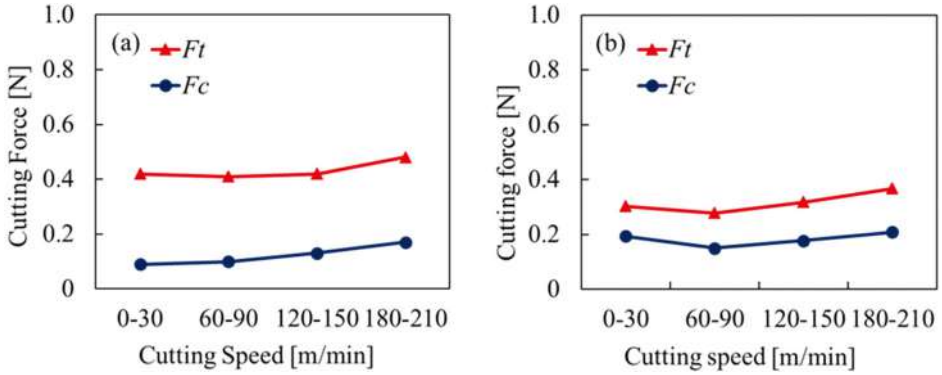

Fig. 9. Cutting forces of PP-CeNF at various cutting speeds and feed rates: (a) $f = 5$ μm/rev; (b) $f = 30$ μm/rev (F_c: principal force, F_t: thrust force).

roughness at a smaller feed rate was smaller than that at a larger feed rate under the same cutting speed.

For the machined surface of pure PP, for both feed rates of 5 and 30 μm/rev, the surface roughness suddenly increased at a high cutting speed (180–210 m/min), while the surface roughness at lower cutting speeds remained at a low level. This indicates that there is a critical cutting speed of approximately 150–180 m/min, beyond which surface tearing becomes significant, as shown in **Fig. 3**.

For the machined surface of PP-CeNF, it was found that under a large feed rate, the surface roughness gradually increased with the cutting speed, whereas under a small feed rate, the surface roughness is hardly affected by the cutting speed. At a high feed rate, CeNFs are pulled out more easily from the matrix, causing tearing of the machined surface. In addition, the plastic flow of the PP matrix was promoted, resulting in waviness on the machined surface. At a low feed rate, however, the surface roughness of PP-CeNF remained almost constant despite the change in cutting speed, and the surface roughness of PP-CeNF was lower than that of pure PP.

3.3. Cutting Force

Figures 8(a) and **(b)** show the cutting forces of pure PP at different cutting speeds and tool feed rates. In all cases, the principal cutting force (F_c) is larger than the thrust force (F_t). Under a small feed rate, F_c and F_t are almost at the same level and do not show obvious changes with cutting speed (**Fig. 8(a)**). However, under a large feed rate, both F_c and F_t increased with the cutting speed (**Fig. 8(b)**).

At a low cutting speed, the plastic deformation of PP in the shear zone dominates the material removal when the undeformed chip thickness is small. However, at a large undeformed chip thickness, PP may behave as a brittle material, and cracks are generated, similar to the cutting phenomenon reported in diamond turning of photoresist [21]; thus, the cutting force becomes much lower. The increase in the cutting force at a high cutting speed might be due to the low-stress relaxation speed of PP compared with the cutting speed. That is, stress relaxation occurs at a lower speed than the strain rate, which is determined by the cutting speed; thus, plastic deformation of the workpiece in the shear zone is less likely to occur uniformly, resulting in unstable surface tearing. Under such a situation, the material is hardened by a high strain rate, leading to a high cutting force. A similar phenomenon has also been reported in cutting polycarbonate and polyester, which have thermoplastic properties similar to those of PP. The cutting forces increase when the cutting speeds gradually increase to ∼40 m/min and ∼3 m/min, respectively [25].

Figures 9(a) and **(b)** show the cutting force of PP-CeNF at different cutting speeds under feed rates of

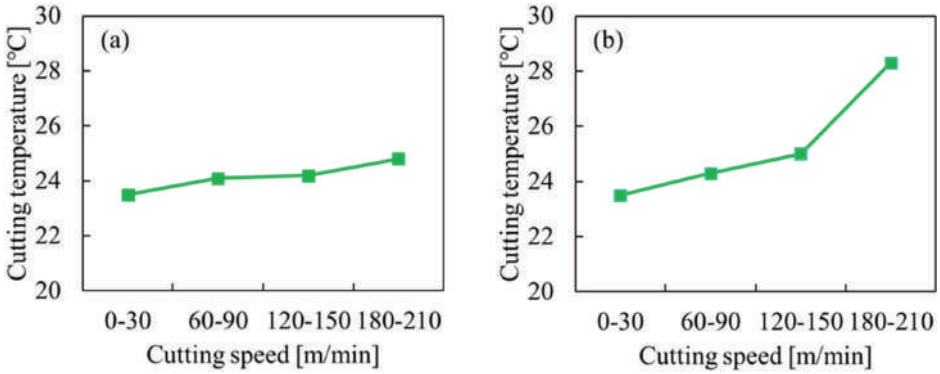

Fig. 10. Cutting temperature of pure PP at various cutting speeds and feed rates: (a) $f = 5$ μm/rev; (b) $f = 30$ μm/rev.

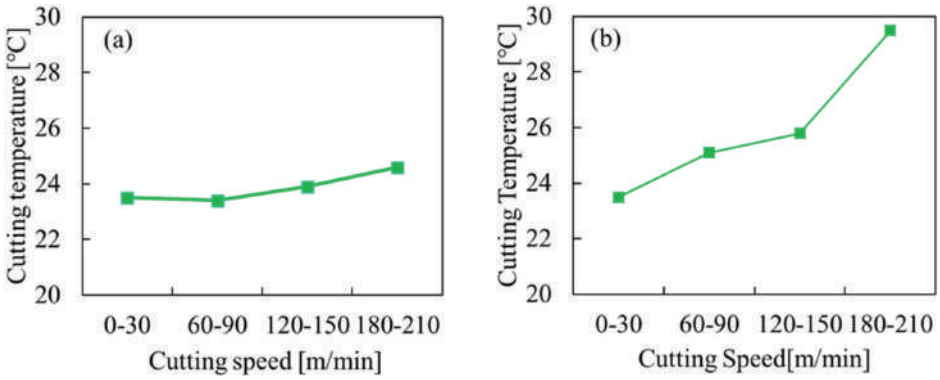

Fig. 11. Cutting temperature of PP-CeNF at various cutting speeds and feed rates: (a) $f = 5$ μm/rev; (b) $f = 30$ μm/rev.

5 and 30 μm/rev, respectively. It is observed that in all cases, the thrust force (F_t) is larger than the principal cutting force (F_c), the tendency of which is opposite to that in **Fig. 8**. This might be because the elasticity of PP-CeNF is larger than that of pure PP owing to the reinforcement effect of the CeNFs. In addition, the difference between F_t and F_c at a feed rate of 5 μm/rev was larger than that at 30 μm/rev. This might be due to the following reasons. At a feed rate of 30 μm/rev, a large amount of CeNFs is pulled out during the removal of the PP matrix, as observed in **Fig. 4**, where tearing and holes are generated on the machine surface. This causes a pulling force in the reverse direction of the thrust force. In contrast, at a feed rate of 5 μm/rev, most CeNFs in the matrix are compressed and bent, as shown in **Figs. 4(a)** and **(c)**, where there are very few tearing and micro-holes on the machine surface [26]. Therefore, the elastic recovery of the machined surface occurs at a much greater extent at a feed rate of 5 μm/rev, resulting in a larger thrust force.

After a comparison between the cutting forces of pure PP and PP-CeNF, it was found that the F_c of PP-CeNF was significantly lower than that of pure PP. This might be the result of the low friction coefficient between the CeNFs and tool surface during the cutting of PP-CeNF. The material removal mechanism of PP-CeNF will be discussed in detail in Section 3.5.

3.4. Cutting Temperature

Figure 10 shows the changes in cutting temperature with cutting speed during the cutting of pure PP. At a low feed rate, the cutting temperature increased slightly with the cutting speed (**Fig. 10(a)**). At a high feed rate (**Fig. 10(b)**), the cutting temperature gradually increased from room temperature with the cutting speed until $V =$ 120–150 m/min. As the cutting speed increased further, the cutting temperature increased rapidly to $\sim$28°C. The tendency to change the cutting temperature is consistent with that of the surface roughness, which confirms that the critical cutting speed is approximately 150–180 m/min. Beyond this critical cutting speed, the PP matrix undergoes viscoelastic/plastic flow, which induces tearing of the machined surface.

Figure 11 shows the changes in cutting temperature with cutting speed during the cutting of PP-CeNF. The trend of temperature changes in cutting PP-CeNF was similar to that in cutting pure PP under both feed rates. An increase in cutting temperature with cutting speed has also been reported for CFRP and GFRP [27, 28]. Under a small feed rate, the measured temperature of PP-CeNF was slightly lower than that of pure PP. This might be caused by two reasons: one is that CeNFs can disperse heat to the surrounding matrix owing to their high thermal conductivity, and the other is the low friction coefficient between the tool surface and the CeNFs, as mentioned in Section 3.3, which reduces both heat generation and cut-

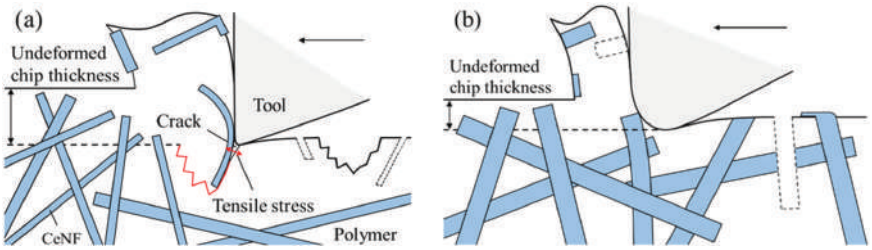

Fig. 12. Cutting model of PP-CeNF: (a) at a large undeformed chip thickness; (b) at a small undeformed chip thickness.

ting forces.

For both pure PP and PP-CeNF, as the cutting speed increases, the slope of the cutting temperature curve at a high feed rate becomes greater than that at a low feed rate. This may be because the contact area between the tool rake face and the chip becomes larger at a higher feed rate. Thus, apart from the heat generated by the deformation of the material in the shear zone ahead of the cutting edge, the heat generated by the friction between the chip and tool rake face also increased sharply at a high cutting speed.

It should be noted that the temperature measured by thermography might be slightly lower than the actual temperature of the cutting region because thermographic temperature measurement is non-invasive and involves complicated error sources. However, the temperature measurement results indicate that the cutting temperature is significantly lower than the softening point of PP (100°C–140°C); thus, the thermally induced softening of PP is not a dominant factor during cutting.

3.5. Material Removal Mechanisms

The above experimental results demonstrate that the tool feed rate is a dominant factor affecting the machined surface quality of PP-CeNF. According to Eq. (1), the maximum undeformed chip thickness $h_{\max}$ at feed rates of 5 and 30 μm/rev were 222 and 1296 nm, respectively. Therefore, the length of the CeNFs embedded in the chip increased with the tool feed rate. For some CeNFs, the embedding length in the chip was larger than that in the workpiece material. This situation makes it easy for the CeNFs to be pulled out from the workpiece surface and removed with the chip, as schematically shown in **Fig. 12(a)**. When a CeNF is pulled out from the workpiece surface, violent tensile stress occurs below the tool tip, which leads to crack initiation in the PP matrix [29]. Meanwhile, owing to the strong adhesion/friction force between the CeNF and PP matrix, many PP matrix materials are removed from the CeNF. As a result, surface tearing is generated on the machined surface of PP-CeNF.

However, when the feed rate was small, the undeformed chip thickness was also small. Thus, the length of the fiber inside the chips is short, which allows the fiber to be pulled out from the chips, resulting in the generation of holes on the cutting chips, as schematically shown in **Fig. 12(b)**. Because the tensile stress in the PP matrix below the tool tip is suppressed at a small undeformed chip thickness owing to the negative effective rake angle, cracks are less likely to occur. The CeNFs were mainly embedded inside the matrix by compressive stress. Owing to the burnishing effect of the tool edge, the removal of CeNFs and surface tearing are greatly suppressed. Therefore, the machined surface of the workpiece became smooth. The above explanation agrees well with the experimental results shown in **Fig. 4**.

4. Conclusions

Pure homogeneous polypropylene (PP) and PP containing cellulose nanofibers (PP-CeNF) were machined under various conditions by ultraprecision diamond turning. The results were compared, and the material removal mechanisms were investigated. The major conclusions are as follows.

(1) The major surface defects in pure PP cutting were surface tearing, which increased with the cutting speed. In contrast, the surface defects in PP-CeNF cutting were tearing and micro-holes induced by the pulling-outs of CeNFs; the latter was independent of cutting speed but affected by the tool feed rate.

(2) When a large feed rate was used (30 μm/rev) to cut PP-CeNF, the surface roughness increased to ~30 nm *Ra* with surface tearing and micro-holes. However, when a small feed rate was used (5 μm/rev), a smooth surface of ~10 nm *Ra* was obtained.

(3) Ribbon-like continuous chips were generated by cutting both pure PP and PP-CeNF. The chip of PP-CeNF generated under a small feed rate featured micro-holes with diameters of tens of nanometers, while under a large feed rate, cellulose nanofibers were observed on the chip surface.

(4) The thrust force was larger than the principal cutting force when cutting the PP-CeNF, whereas a reverse trend was observed when cutting pure PP.

(5) Thermally-induced material softening was not detected in the experiment, whereas strain-rate-induced material hardening was confirmed for both workpiece materials.

References:
[1] H. Yano, "Production of Cellulose Nanofiber Reinforced Optically Transparent Film and Its Properties," J. of the Adhesion Society of Japan, Vol.47, No.5, pp. 210-214, 2011.
[2] H. Yano, "Basics and Applications of Cellulose Materials III: Cellulosic Nanocomposites," J. of the Society of Materials Science, Vol.57, No.3, pp. 310-315, 2008.
[3] T. Saito et al., "An Ultrastrong Nanofibrillar Biomaterial: The Strength of Single Cellulose Nanofibrils Revealed via Sonication-Induced Fragmentation," Biomacromolecules, Vol.14, No.1, pp. 248-253, 2013.
[4] T. Nishino, M. Kotera, and M. Kimoto, "Temperature dependence of the elastic modulus of the crystalline regions of cellulose," Proc. 2nd Int. Cellulose Conf., 2007.
[5] T. Nishino, and T. Peijs, "All-cellulose composites," K. Oksman et al. (Eds.), "Handbook of Green Materials," pp. 201-216, World Scientific, 2014.
[6] A. N. Nakagaito and H. Yano, "The effect of morphological changes from pulp fiber towards nano-scale fibrillated cellulose on the mechanical properties of high-strength plant fiber based composites," Applied Phisics A, Vol.78, No.4, pp. 547-552, 2004.
[7] J. C. Lee, J. A. Lee, D. Y. Lim, and K. Y. Kim, "Fabrication of Cellulose Nanofiber Reinforced Thermoplastic Composites," Fibers and Polymers, Vol.19, pp. 1753-1759, 2018.
[8] M. Nogi et al., "Optically transparent bionanofiber composites with low sensitivity to refractive index of the polymer matrix," Applied Physics Letters, Vol.87, 243110, 2005.
[9] S. Fujisawa et al., "Comparison of mechanical reinforcement effects of surface modified cellulose nanofibrils and carbon nanotubes in PLLA composites," Composites Science and Technology, No.90, pp. 96-101, 2014.
[10] A. Isogai, M. Kawasaki, and H. Yano, "Technical Data of Cellulose Nanofibers," CMC Publishing Co., Ltd., 2016 (in Japanse).
[11] L. Wang, K. Okada, M. Sodenaga, Y. Hikima, M. Ohshima, T. Sekiguchi, and H. Yano, "Effect of surface modification on the dispersion, rheological behavior, crystallization kinetics, and foaming ability of polypropylene/cellulose nanofiber nanocomposites," Composites Science and Technology, Vol.168, pp. 412-419, 2018.
[12] L. Wang, M. Ando, M. Kubota, S. Ishihara, Y. Hikima, M. Ohshima, T. Sekiguchi, A. Sato, and H. Yano, "Effects of hydrophobic-modified cellulose nanofibers (CNFs) on cell morphology and mechanical properties of high void fraction polypropylene nanocomposite foams," Compos. Part A, Vol.98, No.C, pp. 166-173, 2017.
[13] B. Yan, Y. Huang, and S. Yeh, "The effect of fiber angles on the machinability of CFRP," Japan Society for Precision Engineering, Spring 2, pp. 719-720, 1991.
[14] T. Kaneeda, "CFRP Cutting Mechanism (3rd Report) – Effects of Tool Edge Roundness and Relief Angle on Cutting Phenomena –," J. of the Japan Society for Precision Engineering, Vol.57, No.3, pp. 491-496, 1991.
[15] W. Huang and J. Yan, "Surface formation mechanism in ultraprecision diamond turning of coarse-grained polycrystalline ZnSe," Int. J. of Machine Tools and Manufacture, Vol.153, 103554, 2020.
[16] M. Heidari, J. Akbari, and J. Yan, "Effects of tool rake angle and tool nose radius on surface quality of ultraprecision diamond-turned porous silicon," J. of Manufacturing Processes, Vol.37, pp. 321-331, 2019.
[17] K. Q. Xiao and L. C. Zhang, "The role of viscous deformation in the machining of polymers," Int. J. of Mechanical Sciences, Vol.44, No.11, pp. 2317-2336, 2002.
[18] Y. C. Jean (Ed.), "Positron and Positronium Chemistry," World Scientific, 1990.
[19] R. F. Boyer, "Transitions and Relaxation," H. F. Mark and N. M. Bikales (Eds.), "Encyclopedia of Polymer Science and Technology," Supplement Vol.2, Wiley, 1997.
[20] A. Uedono and S. Tanigawa, "Glass Transition and Relaxation Processes of Polymers Studied by Positron Annihilation," Japanese J. of Polymer Science and Technology, Vol.53, No.10, pp. 563-574, 1996.
[21] J. Yan, "Ultraprecision cutting of photoresist/gold composite microstructures," CIRP Annals, Vol.60, No.1, pp. 133-136, 2011.
[22] J. Carr and C. Feger, "Ultraprecision machining of polymers," Precision Engineering, Vol.15, No.4, pp. 221-237, 1993.
[23] H. J. Yoon, B. M. Gil, J. H. Lee et al., "Thermal and Mechanical Properties of Polypropylene/Cellulose Nanofiber Composites," Polymer-Korea, Vol.44, pp. 255-263, 2020.
[24] H. Kurita, R. Ishigami, C. Wu, and F. Narita, "Experimental Evaluation of Tensile Properties of Epoxy Composites with Added Cellulose Nanofiber Slurry," Strength of Materials, Vol.52, No.5, pp. 798-804, 2020.
[25] A. Kobayashi and K. Saito, "On the cutting mechanism of plastics," CIRP Annals, Vol.11, pp. 82-89, 1962.
[26] T. Kaneeda and M. Takahashi, "CFRP cutting mechanism (2nd report) – Analysis of depth of reluctant uncut and deformed part –," J. of the Japan Society for Precision Engineering, Vol.56, No.6, pp. 1058-1063, 1990.
[27] P. S. Sreejith, R. Krishnamurthy, S. K. Malhotra, and K. Narayanasamy, "Evaluation of PCD tool performance during machining of carbon/phenolic ablative composites," J. of Materials Processing Technology, Vol.104, No.1-2, pp. 53-58, 2000.
[28] K. Sakuma and M. Seto, "Tool wear in cutting glass-fiber-reinforced-plastics: The relation between cutting temperature and tool wear," Bulletin of JSME, Vol.24, No,190, pp. 748-755, 1981.
[29] J. Yan, K. Syoji, T. Kuriyagawa, and H. Suzuki, "Ductile regime turning at large tool feed," J. of Materials Processing Technology, Vol.121, No.2-3, pp. 363-372, 2002.

Name:
Yu Kamada

Affiliation:
Master Course Student, Graduate School of Science and Technology, Keio University

Address:
3-14-1 Hiyoshi, Kohoku-ku, Yokohama, Kanagawa 223-8522, Japan

Brief Biographical History:
2019- Graduate School of Science and Technology, Keio University

Name:
Jiwang Yan

Affiliation:
Professor, Department of Mechanical Engineering, Faculty of Science and Technology, Keio University

Address:
3-14-1 Hiyoshi, Kohoku-ku, Yokohama, Kanagawa 223-8522, Japan

Brief Biographical History:
1987-1994 B.E./M.E. Candidate, Jilin University
1994-1996 Ph.D. Candidate, Tsinghua University
1996-2000 Ph.D. Candidate, Tohoku University
2000-2001 Research Associate, Tohoku University
2001-2005 Associate Professor, Kitami Institute of Technology
2005-2012 Associate Professor, Tohoku University
2012- Professor, Keio University

Main Works:
• J. Yan (Ed.), "Micro and Nano Fabrication Technology," Springer Nature, 2018.
• J. Yan and N. Takayama, "Micro and Nanoscale Laser Processing of Hard Brittle Materials," Elsevier, 2019.

Membership in Academic Societies:
• Japan Society of Mechanical Engineers (JSME)
• Japan Society for Precision Engineering (JSPE)
• Japan Society for Abrasive Technology (JSAT)
• Japan Society of Applied Physics (JSAP)
• American Society for Precision Engineering (ASPE)
• European Society for Precision Engineering and Nanotechnology (euspen)
• International Academy for Production Engineering (CIRP)